


Analysis of multinucleon transfer reactions with spherical and statically deformed nuclei using a Langevin-type approach

V. V. Saiko and A. V. Karpov*

*Flerov Laboratory of Nuclear Reactions, JINR, 141980 Dubna, Russia
and Department of Nuclear Physics, Dubna State University, 141982 Dubna, Russia*

 (Received 4 June 2018; revised manuscript received 26 November 2018; published 15 January 2019)

Background: In recent years, there has been increasing interest in multinucleon transfer processes in low-energy deep inelastic (damped) collisions of heavy ions. Partly, it was provoked by a possibility of using them as a method of production of heavy neutron-enriched nuclei. Possible promising projectile-target combinations include nuclei deformed in the ground state (e.g., actinides). Mutual orientations of such nuclei in the entrance channel of a reaction may significantly influence the reaction dynamics.

Purpose: The major aim of the work is to implement a possibility of modeling collisions of statically deformed heavy nuclei within a multidimensional dynamical model based on the Langevin equations. Another purpose of the paper is to study the influence of mutual orientations of statically deformed nuclei on their collision dynamics. Finally, production yields of heavy transuranium nuclei in collisions of actinides are examined.

Method: An analysis has been performed within a multidimensional dynamical model of nucleus-nucleus collisions based on the Langevin equations [*Phys. Rev. C* **96** 024618 (2017)]. In the present paper, the model has been improved to describe collisions of statically deformed heavy nuclei with different mutual orientations.

Results: The available experimental data on multinucleon transfer reactions with statically deformed as well as spherical heavy nuclei $^{144}\text{Sm} + ^{144}\text{Sm}$, $^{154}\text{Sm} + ^{154}\text{Sm}$, $^{160}\text{Gd} + ^{186}\text{W}$, and $^{208}\text{Pb} + ^{208}\text{Pb}$, ^{238}U have been analyzed within the developed model. A good agreement of the calculated quantities with the corresponding experimental data has been reached. Special attention in the paper is paid to analyzing the possibility of producing neutron-enriched isotopes of heavy and superheavy elements in multinucleon transfer processes in $^{238}\text{U} + ^{238}\text{U}$, ^{248}Cm , ^{254}Es collisions.

Conclusions: Mutual orientation of colliding statically deformed nuclei in the entrance channel strongly affects the energy, angular, mass, and charge characteristics of multinucleon transfer reaction products at near-barrier energies. These orientational effects disappear with increasing collision energy well above the Coulomb barrier. An exponential drop in the isotopic distributions of the above-target products formed in the collisions of actinides with an increasing atomic number does not allow one to synthesize new isotopes of superheavy nuclei with experimentally reachable cross sections. However, there is a possibility to produce a number of neutron-enriched isotopes of heavy actinides with cross sections exceeding $1 \mu\text{b}$.

DOI: [10.1103/PhysRevC.99.014613](https://doi.org/10.1103/PhysRevC.99.014613)

I. MOTIVATION

Intensive nucleon transfer between interacting nuclei may occur in quasifission and deep inelastic (DI) collisions of heavy ions. This feature of DI collisions has already been used to synthesize several light neutron-enriched nuclides shortly after the discovery of this type of nuclear reactions [1]. Nowadays, the possibility of producing neutron-enriched isotopes of heavy elements in these reactions is widely discussed [2–7]. The recent experiments have confirmed applicability of this method [8–11] in spite of the fact that proper separation of heavy nuclides from all multinucleon transfer (MNT) reaction products in a wide range of masses and kinetic energies still remains a challenging task.

Investigation of heavy neutron-rich nuclei in the vicinity of the $N = 126$ neutron shell closure and study of their proper-

ties are of great interest, first of all, due to their influence on the problem of origination of chemical elements heavier than iron in the r -process of astrophysical nucleosynthesis. The possibility of synthesizing neutron-rich nuclei with $N = 126$ has been analyzed in our earlier paper [7], where certain promising combinations of heavy nuclei were investigated within a multidimensional dynamical model based on the Langevin equations. A reasonable agreement with the available experimental data on angular, energy, mass, and charge distributions of MNT reaction products has been achieved. Cross sections for production of nuclei with $N = 126$ have been predicted in a wide range of collision energies.

The systems studied in Ref. [7] involved heavy nuclei having spherical shapes in the ground state. However, collisions of heavy statically deformed nuclei are of particular interest as well. First, mutual orientation of the reaction partners influences the collision dynamics. There are several indications that the orientation of colliding nuclei at the contact point strongly affects the probability of formation of a compound

*karpov@jinr.ru

nucleus in fusion reactions [12–15]. This probability significantly decreases for nose-to-nose orientations, which leads to decay of the nuclear system primarily in quasifission channels. Second, collisions of deformed nuclei can be used for synthesis of new heavy or even superheavy neutron-enriched nuclei. For example, a possibility of production of neutron-rich nuclei in the vicinity of the $N = 126$ shell closure in the reaction of two statically deformed nuclei $^{160}\text{Gd} + ^{186}\text{W}$ has been predicted in Ref. [4]. The orientational effects for this system of nuclei have recently been studied experimentally in Ref. [11] and theoretically in Ref. [16].

Actinides are a particular example of statically deformed nuclei. Obviously, formation of a compound nucleus is impossible in reactions between them. However, these reactions may lead to formation of neutron-enriched heavy and superheavy nuclei in DI collisions, if the contact time of two nuclei is sufficient to transfer a large number of nucleons. It may give one a possibility of producing several new neutron-enriched isotopes of transuranium elements with rather large cross sections. The yields of heavy nuclei up to mendelevium have been measured in the $^{238}\text{U} + ^{238}\text{U}$, ^{248}Cm reactions by radiochemical methods in Refs. [17,18]. Dynamics of $^{238}\text{U} + ^{238}\text{U}$ collisions has been studied experimentally in Ref. [19]. Extensive theoretical investigations of the collisions of actinides performed in the works of Zagrebaev and Greiner [5,20] have shown that strong shell effects in the potential energy of the nuclear system favor the formation of the first fragment in the region of doubly magic lead and the second one in the region of superheavy elements. Moreover, the potential energy structure favors the formation of neutron-enriched nuclei unreachable in fusion reactions of stable nuclei. Recently, this problem has also been investigated in Refs. [21,22] within an improved quantum molecular dynamics model, as well as in Ref. [23] within a dinuclear system model.

Consideration of orientational degrees of freedom in dynamical calculations within any model using the concept of nuclear shape is quite a complicated problem and has no straightforward solution yet. Reasonable assumptions should be made in order to avoid any major difficulties. The main problem here is to calculate the potential energy corresponding to sequential shapes of the nuclear system, which are unknown in the absence of the axial symmetry. In particular, it concerns restoration of the axial symmetry of two arbitrary oriented nuclei at the contact point.

Thus, the first aim of this work is to advance the model developed recently in Ref. [7] in order to simulate collisions of heavy statically deformed nuclei. The second purpose of the paper is to study the impact of mutual orientations of statically deformed nuclei on their collision dynamics. Finally, the production yields of heavy transuranium nuclei in collisions of actinides are examined.

II. MODEL

The model has been described in detail in Ref. [7]. Here we provide only its basics. The model has eight degrees of freedom describing a system of two colliding nuclei. Four of them originate from the well-known two-center shell model (TCSM) parametrization [24] and define the nuclear shape:

distance r between the geometrical centers of two nuclei, two independent ellipsoidal surface deformations $\delta_{1,2}$, and mass asymmetry η_A . In addition, charge asymmetry η_Z is included in the model, which allows us to describe independent proton and neutron transfer and production of nuclei with different atomic and mass numbers. Two angles $\varphi_{1,2}$ of rotation of the projectile and target nuclei and angle θ between the internuclear axis and the beam direction are included in the model as well.

A set of eight coupled Langevin equations is solved numerically:

$$\begin{aligned} \dot{q}_i &= \sum_j \mu_{ij} p_j, \\ \dot{p}_i &= T \left(\frac{\partial S}{\partial q_i} \right)_{E_{\text{tot}}} - \sum_{j,k} \gamma_{ij} \mu_{jk} p_k + \sum_j \theta_{ij} \xi_j(t), \end{aligned} \quad (1)$$

where $q_i = \{r, \delta_1, \delta_2, \eta_A, \eta_Z, \theta, \varphi_1, \varphi_2\}$ and $p = \{p_r, p_{\delta_1}, p_{\delta_2}, p_{\eta_A}, p_{\eta_Z}, L, l_1, l_2\}$ are the collective degrees of freedom and their conjugate momenta, respectively. $S = 2\sqrt{aE^*}$ is the entropy of an excited system, where a is the level-density parameter and $E^* = E_{\text{tot}} - V - E_{\text{kin}}$ is the excitation energy. Here E_{tot} is the total energy of the system, E_{kin} is the kinetic energy stored in all collective degrees of freedom, and V is the potential energy. $\mu_{ij} = [m_{ij}]^{-1}$ is the inverse inertia tensor, γ_{ij} is the friction tensor, θ_{ij} are the amplitudes of the random forces determined from the Einstein equation $\theta_{ik}\theta_{kj} = \gamma_{ij}T$, ξ_i are the normalized random variables with Gaussian distribution $\langle \xi_i(t) \rangle = 0$, $\langle \xi_i(t), \xi_j(t') \rangle = 2\delta_{ij}\delta(t-t')$, and $T = \sqrt{E^*/a}$ is the nuclear temperature. The terms in Eq. (1) represent the driving, friction, and random forces, respectively.

It is well known [25,26] that for excited nuclear systems one should use a thermodynamic potential (e.g., the entropy or free energy) instead of a bare potential in order to determine the driving force entering the Langevin equations. In particular, in the present model the driving force is given by the derivative of the entropy with respect to the collective coordinates at the constant total energy: $T(\partial S/\partial q_i)_{E_{\text{tot}}}$. It is easy to see that the driving force consists of the usual conservative force $-\partial V/\partial q_i - 1/2 \sum_j p_j p_j \partial \mu_{ij}/\partial q_i$ plus a term that comes from the thermodynamic properties of the excited nuclear system, which enters via the derivative of the level-density parameter a as: $T^2 \partial a/\partial q_i$. Note also that since the entropy $S \sim \ln \rho$, the driving force is related to the derivative of the density of excited states ρ .

Potential energy, friction, and inertia coefficients are the main values that govern the evolution of the nuclear system. We calculate them on a grid before starting the dynamical calculations. The multidimensional potential energy takes into account transition from the diabatic regime of nuclear motion to the adiabatic one as a relaxation process with the relaxation time τ_{DA} :

$$\begin{aligned} V(r, \delta_1, \delta_2, \eta_A, \eta_Z; t) \\ = V_{\text{diab}} \exp\left(-\frac{t}{\tau_{\text{DA}}}\right) + V_{\text{adiab}} \left[1 - \exp\left(-\frac{t}{\tau_{\text{DA}}}\right)\right]. \end{aligned} \quad (2)$$

The diabatic potential is calculated within the double-folding method with Migdal nucleon-nucleon forces [27]. An extended macromicroscopic approach [28,29] is used to calculate the adiabatic potential:

$$V_{\text{adiab}}(r, \delta_1, \delta_2, \eta_A, \eta_Z) = V_{\text{mac}}(r, \delta_1, \delta_2, \eta_A, \eta_Z) + \delta E(r, \delta_1, \delta_2, \eta_A, \eta_Z),$$

where the macroscopic term V_{mac} is calculated within the finite-range liquid-drop model [30], and δE is the shell correction calculated based on the Strutinsky method [31,32].

We calculate the inertia coefficients for the $r, \delta_1, \delta_2, \eta_A$ degrees of freedom according to the Werner-Wheeler approach for an incompressible irrotational flow [33]. The corresponding friction coefficients are evaluated within the ‘‘wall+window’’ mechanism of one-body dissipation [34]. The inertia and friction coefficients for the charge asymmetry are calculated in the same manner as in Ref. [35].

There is a number of important peculiarities of treating nuclear motion for the system of two separated nuclei. The inertia and the friction tensors are diagonal in this case. The Werner-Wheeler approach and the model of one-body dissipation can still be used for deformation degrees of freedom δ_1 and δ_2 . For relative motion, the inertia coefficient m_{rr} is equal to the reduced mass of the system. All other transport coefficients $\mu_{\eta_A\eta_A}, \mu_{\eta_Z\eta_Z}, \gamma_{rr}, \gamma_{\eta_A\eta_A},$ and $\gamma_{\eta_Z\eta_Z}$ are zero for separated nuclei calculated within the models mentioned above. This does not allow one to take into account the fact that dissipation of angular momentum and energy of relative motion starts even before contact, when nuclei approach each other at the distance of nuclear forces range (~ 2 fm), and their diffusenesses overlap. There is also a possibility of nucleon transfer at the approaching stage, which can be modeled within the Langevin-type approach in the presence of nonzero transport coefficients only.

To take into account these effects and following the surface friction model [25], a phenomenological nuclear friction force with a Woods-Saxon-type form factor is included in the model, as suggested in Ref. [36]. This additional form factor $F(r)$ tends to zero in the mononucleus stage, where the one-body friction yields a nonzero dissipation. Thus, the radial friction coefficient γ_{rr} is calculated as a weighted sum of two terms,

$$\gamma_{rr} = w_F(r)\gamma_{rr}^{o.b.} + [1 - w_F(r)]\gamma_r^0 F(r),$$

$$F(r) = \left\{ 1 + \exp\left(\frac{r - R_{\text{contact}} - \Delta R_F}{a_F}\right) \right\}^{-1}, \quad (3)$$

where $\gamma_{rr}^{o.b.}$ is the friction coefficient according to the model of one-body dissipation, and the weighting function is

$$w_F(r) = \left\{ 1 + \exp\left(\frac{r - R_{\text{contact}} + \Delta R_F}{a_F}\right) \right\}^{-1}. \quad (4)$$

The friction strength γ_r^0 , the friction distance ΔR_F , and the friction diffuseness a_F coefficients are the model parameters. Their values were determined in Ref. [7] by fitting calculations to the experimental data for quasielastic and DI scattering. The most sensitive quantities to these parameters are the grazing angle of the collision and the slope and lowest value of

the quasielastic part of the fragment energy distribution. The following values were determined: $\gamma_r^0 = 30 \times 10^{-22}$ MeV s fm $^{-2}$, $\Delta R_F = 2.5$ fm, and $a_F = 0.2$ fm.

It can be shown that the friction coefficients for the mass and charge asymmetries for separated nuclei are related to the corresponding transfer rates as

$$\gamma_{\eta_x\eta_x} = \frac{T}{\lambda_{\eta_x}} \frac{1}{R_0^2}, \quad x = A, Z, \quad (5)$$

where R_0^2 is the dimension factor and the quantity λ_{η_x} can be calculated as (see Eq. (5) in Ref. [36])

$$\lambda_{\eta_A} = \lambda_A^0 P_{\text{tr}}(r) \frac{4}{A^2}, \quad \lambda_{\eta_Z} = \lambda_Z^0 P_{\text{tr}}(r) \frac{4}{A^2} g_{ZA}, \quad (6)$$

where λ_A^0 and λ_Z^0 are the mass and charge transfer rates, and P_{tr} is the probability of nucleon transfer depending on the distance between the nuclear surfaces. The term $A^2/4$ appears, because the mass asymmetry is used as a collective coordinate. The probability P_{tr} goes exponentially to zero at $r \rightarrow \infty$ and is equal to unity for the overlapping nuclei. In the calculations, we use the semiclassical approximation for $P_{\text{tr}} = \exp(-2\kappa\xi)$ proposed in Ref. [37]. Here $\xi = r - R_{\text{contact}} - \Delta R_N$, where $\Delta R_N \simeq \Delta R_F$, i.e., the radius of nucleon transfer coincides with the radius of the radial friction, and $\kappa = \sqrt{2\mu_n B_n/\hbar^2}$, where μ_n is the nucleon reduced mass and B_n is its separation energy. Again, for continuity, the friction coefficients for the mass and charge asymmetries for separated nuclei and the mononucleus are joined in the vicinity of the contact point. It is assumed that $\lambda_A^0 = \lambda_Z^0$, and the ratio $g_{ZA} = \lambda_{\eta_Z}/\lambda_{\eta_A}$ is the same as given by the corresponding window formulas (close to unity). Thus, we have one free parameter λ_A^0 which was determined in Ref. [7] as $1(T/\text{MeV}) \times 10^{22}$ s $^{-1}$. The corresponding inverse inertia coefficients $\mu_{\eta_A\eta_A}$ and $\mu_{\eta_Z\eta_Z}$ for separated nuclei are estimated, assuming that the damping coefficients $\gamma_{\eta_x\eta_x}\mu_{\eta_x\eta_x}$ have the same values as those calculated with the one-body friction and hydrodynamical masses in the vicinity of the contact point. The values of $\mu_{\eta_A\eta_A}$ and $\mu_{\eta_Z\eta_Z}$ are close to each other and equal to approximately $0.005 R_0^{-2} m_N^{-1}$.

The solution of Eq. (1) starts from the initial distance between nuclei ≈ 50 fm. A projectile with a given impact parameter b and a certain center-of-mass energy $E_{\text{c.m.}}$ approaches a target nucleus. The nucleon transfer and energy dissipation processes start to occur slightly before the nuclei come into contact. Then the dinuclear system forms and decays into two excited reaction fragments. The calculations are terminated when the products are formed and separated again by the initial distance (≈ 50 fm). The obtained solution is a trajectory in the multidimensional space of the collective degrees of freedom that carry complete information about a single collision.

A large number of trajectories for different impact parameters are simulated. For each solution of the dynamical equations, one knows such characteristics of primary fragments, as their masses, atomic numbers, excitation energies, angular momenta, angles of reparation, kinetic energies, etc. Then the statistical model [7,29,38,39] is used to obtain the characteristics of the final reaction products. The statistical

model takes into account evaporation of neutrons, protons, α particles, and γ quanta, as well as fission of an excited nucleus. Decay of each fragment is considered independently. It is also assumed that particle evaporation does not alter the fragment emission angles and velocities. Usually the Monte Carlo method (see Ref. [7] for details) of simulation is used, but for highly fissile reaction products the method of nested integrals (see Ref. [40]) is applied under the assumption that final products are formed in neutron evaporation channels only (up to four neutrons). The GEF code [41] is employed for simulation of sequential fission (SeqF) fragment distribution. The SeqF fragments are assumed to be emitted isotropically in the center-of-mass system of the fissioning nucleus with the total kinetic energy calculated according to the systematics of Ref. [42]. Finally, the cross sections are calculated as

$$\frac{d^4\sigma}{dZdAdEd\Omega}(Z, A, E, \theta) = \int_0^{b_{\max}} \frac{\Delta N(b, Z, A, E, \theta)}{N_{\text{tot}}(b)} \frac{b db}{\Delta Z \Delta A \Delta E \sin \theta \Delta \theta}, \quad (7)$$

where ΔN is the number of trajectories in a given bin and N_{tot} is the total number of simulated trajectories for each impact parameter. Integration of Eq. (7) allows one to obtain different distributions of reaction products.

In order to consider the collisions of statically deformed nuclei, one should take into account that the reaction dynamics is strongly dependent on the mutual orientations of the nuclei. This happens, first of all, because of the change of the potential energy. The orientation effects in the potential energy can be easily considered for separated “frozen” nuclei. In this case, the potential energy is calculated using the double-folding procedure [27]. After the contact, the potential energy depends on the interaction time. In particular, the axial symmetry should be restored if the interaction time is long enough. Another difficulty in calculation of the potential energy of a strongly interacting nuclear system with broken axial symmetry is connected with appearance of dynamical deformations. They should develop predominately along the axis connecting the geometrical centers of the interacting nuclei. This destroys the axial symmetry of each of the reaction partners, which complicates the task even more.

Thus, the sequence of shapes passed by arbitrary oriented colliding nuclei in the vicinity of the contact point is unknown and the calculation of the corresponding potential energy for these shapes with broken axial symmetry is a rather complicated and as yet unsolved problem. It is difficult or even impossible to solve this problem based on the implication of any parametrization of nuclear shape without a substantial increase in the number of degrees of freedom. Finally, one may conclude that a certain approximation should be employed.

Detailed studies within the time-dependent microscopic approaches may shed more light on the problem of evolution of nuclear shapes for arbitrary oriented interacting nuclei. For example, according to time-dependent calculations for the $^{48}\text{Ca} + ^{249}\text{Bk}$ collisions with berkelium orientation of 45° , it takes the dinuclear system about 3×10^{-21} s to restore its axial symmetry [43,44]. We suppose that this time should be close to the period of quadrupole oscillations of an isolated

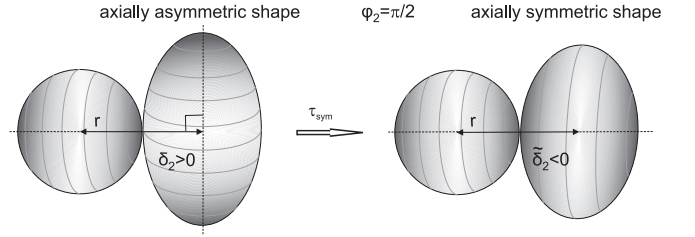


FIG. 1. Example of evolution of an axially asymmetric nuclear system to an axially symmetric one.

nucleus. The corresponding value for the ^{249}Bk nucleus is approximately 6×10^{-21} s, which is in line with this assumption.

It is rather natural to use the exponential factor in order to simulate the process of restoration of axial symmetry in the potential energy. The potential energy is thus calculated as

$$V = V_{\text{asym}} \exp\left(-\frac{t}{\tau_{\text{sym}}}\right) + V_{\text{sym}} \left[1 - \exp\left(-\frac{t}{\tau_{\text{sym}}}\right)\right], \quad (8)$$

where V_{sym} and V_{asym} are the potentials (2) calculated for axially symmetric and axially asymmetric configurations, respectively, and τ_{sym} is the relaxation time. We have found that the value of this relaxation time mainly influences the maximal value of the kinetic energy loss in deep inelastic collisions of heavy ions. Larger values of τ_{sym} lead to smaller maximal kinetic energy losses, because the system experiences over a longer period of time the potential energy for oriented nuclei having a larger barrier than the one for the axially symmetric configuration. The value used in the present calculation was chosen, as described above, to be $\tau_{\text{sym}} = 10^{-21}$ s.

We assume that the relaxation process of an arbitrary oriented nuclear system to an axially symmetric one starts when the colliding nuclei approach the distance of strong interaction (~ 2 fm between the nuclear surfaces). The relaxation process cannot result in an increase in the potential energy of the system. The potential energy of two heavy nuclei at the vicinity of the contact point is mainly determined by the distance between the nuclear surfaces. Thus, we assume that arbitrary oriented nuclei keep the distance between their surfaces (as well as the relative distance r), while the relaxation process proceeds in the perpendicular direction (see Fig. 1). This allows us to relate the ellipsoidal deformations δ_i of an initially oriented pair of colliding nuclei with the ellipsoidal deformations $\tilde{\delta}_i$ of final axially symmetric shapes:

$$\tilde{\delta}_i = (1 + \delta_i)[\delta_i(2 + \delta_i) \sin^2 \varphi_i + 1]^{-\frac{3}{4}} - 1. \quad (9)$$

It is often assumed that initial mutual orientations of colliding nuclei do not change before the nuclei come into contact. This assumption is also used in the present model, which allows us to simplify the consideration of collision dynamics for separated nuclei substantially. However, time evolution of the angles φ_i cannot be ignored completely. In the vicinity of the contact point, sliding friction between nuclear surfaces leads to the so-called dissipation of the angular momentum of relative motion until the sticking condition is reached. A part of the relative angular momentum is thus transferred into

the angular momenta of the reaction partners, which results in time evolution of the angles φ_i , which should be therefore kept in the system of the Langevin equations (1). Such consideration allows us to simulate the nonzero momenta of the reaction products.

To simplify the calculations, we have considered only the limit initial orientations of two deformed colliding nuclei: the so-called tip-to-tip ($\varphi_1^0 = \varphi_2^0 = 0$), side-to-side ($\varphi_1^0 = \varphi_2^0 = \pi/2$), tip-to-side ($\varphi_1^0 = 0, \varphi_2^0 = \pi/2$), and side-to-tip ($\varphi_1^0 = \pi/2, \varphi_2^0 = 0$) collisions. If the orientation of the i th nucleus is $\varphi_i^0 = \pi/2$, the corresponding deformation of the axially symmetric shape has a simple form:

$$\tilde{\delta}_i = (1 + \delta_i)^{-\frac{1}{2}} - 1. \quad (10)$$

Finally, the cross sections are averaged over the initial mutual orientations as

$$\langle \sigma(Z, A, E, \theta) \rangle = \int_0^{\frac{\pi}{2}} \int_0^{\frac{\pi}{2}} \sigma(Z, A, E, \theta, \varphi_1^0, \varphi_2^0) \sin \varphi_1^0 \times \sin \varphi_2^0 d\varphi_1^0 d\varphi_2^0, \quad (11)$$

where the cross section $\sigma(Z, A, E, \theta, \varphi_1^0, \varphi_2^0)$ is calculated at four limit orientations of colliding nuclei $\varphi_i^0 = 0, \pi/2$ and assumed to be linearly dependent on the angles φ_1^0 and φ_2^0 .

III. ANALYSIS OF MULTINUCLEON TRANSFER REACTIONS

In our previous work [7], the developed model was successfully applied to analysis of reaction dynamics and production of heavy neutron-enriched nuclei in MNT reactions with heavy spherical nuclei $^{136}\text{Xe} + ^{198}\text{Pt}$, ^{208}Pb , ^{209}Bi . The present work is devoted to comparison of DI collisions with deformed and spherical nuclei. All the calculations were done within a set of the model parameters fixed in Ref. [7].

Note that the reactions considered in this paper are those between heavy nuclei. They are characterized by strong Coulomb interaction. Therefore, a substantial part of the kinetic energy of relative motion dissipates on the approaching stage of the reaction even before nuclei enter into the region of strong nuclear interaction (~ 2.5 fm between the nuclear surfaces). According to the calculations, the corresponding dissipated energy may constitute a value of up to 40 MeV for central collisions of two uranium nuclei at near-barrier energies and gradually decreases with an increase in the impact parameter. In addition, excitation of collective modes, such as surface vibrations and/or rotations, may occur. This effect is also taken into account by the present model, since the ellipsoidal deformations and angles of orientation of both reaction partners are among the considered collective variables.

The discussion of the studied reactions is ordered by the mass of the composite systems. We demonstrate how accurately the developed model is able to describe various experimental measurable characteristics. The influence of mutual orientation of statically deformed nuclei on these characteristics is also discussed. Finally, we analyze a possibility of production of neutron-enriched transuranium nuclides in low-energy collisions of actinides.

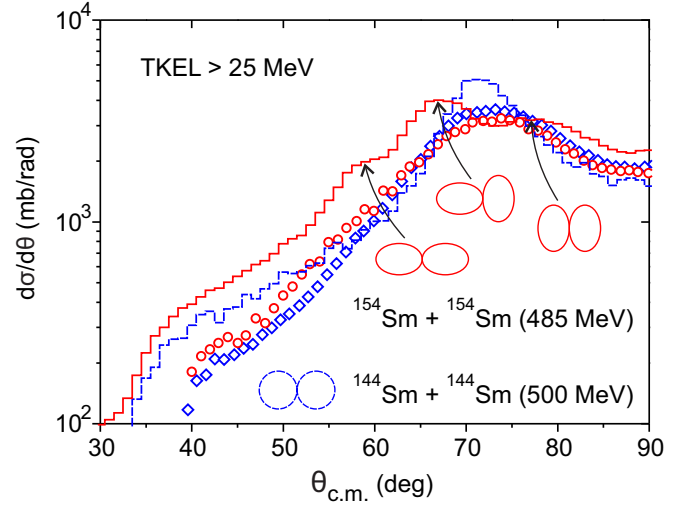


FIG. 2. Angular distributions of reaction products with TKEL > 25 MeV obtained in the $^{144}\text{Sm} + ^{144}\text{Sm}$ and $^{154}\text{Sm} + ^{154}\text{Sm}$ reactions at energies $E_{\text{c.m.}} = 500$ and 485 MeV, respectively. The histograms are the calculation results and the symbols show the experimental data [46]. The dashed histogram and diamonds correspond to the $^{144}\text{Sm} + ^{144}\text{Sm}$ reaction. The solid histogram and circles illustrate the $^{154}\text{Sm} + ^{154}\text{Sm}$ reaction.

A. $^{144}\text{Sm} + ^{144}\text{Sm}$ and $^{154}\text{Sm} + ^{154}\text{Sm}$ systems

The first combination consists of spherical magic nuclei [$\beta_2(^{144}\text{Sm}) = 0$], while the second one involves well-deformed nuclei ($\beta_2(^{154}\text{Sm}) = 0.27$ [30]). These two reactions are of particular interest, because they allow us to study

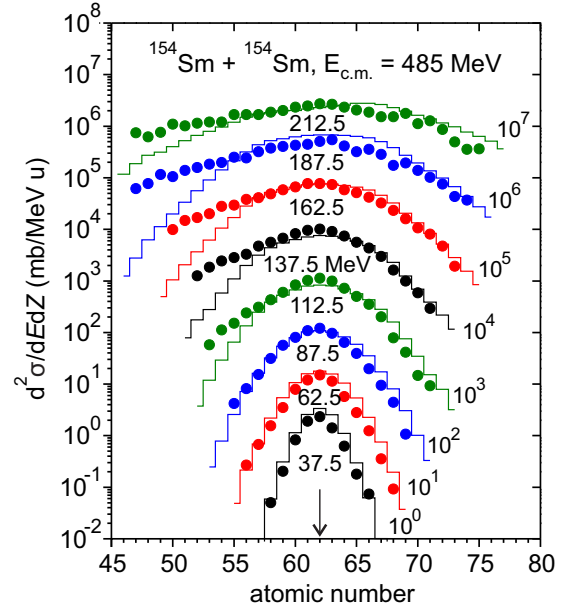


FIG. 3. Charge distributions of final products for different values of TKEL obtained in the $^{154}\text{Sm} + ^{154}\text{Sm}$ reaction at $E_{\text{c.m.}} = 485$ MeV. The energy bins are 25 MeV wide. The midpoints of each bin are indicated. Both experimental (symbols) and calculated (histograms) data were multiplied by the factors indicated on the side. The experimental data are from Ref. [46].

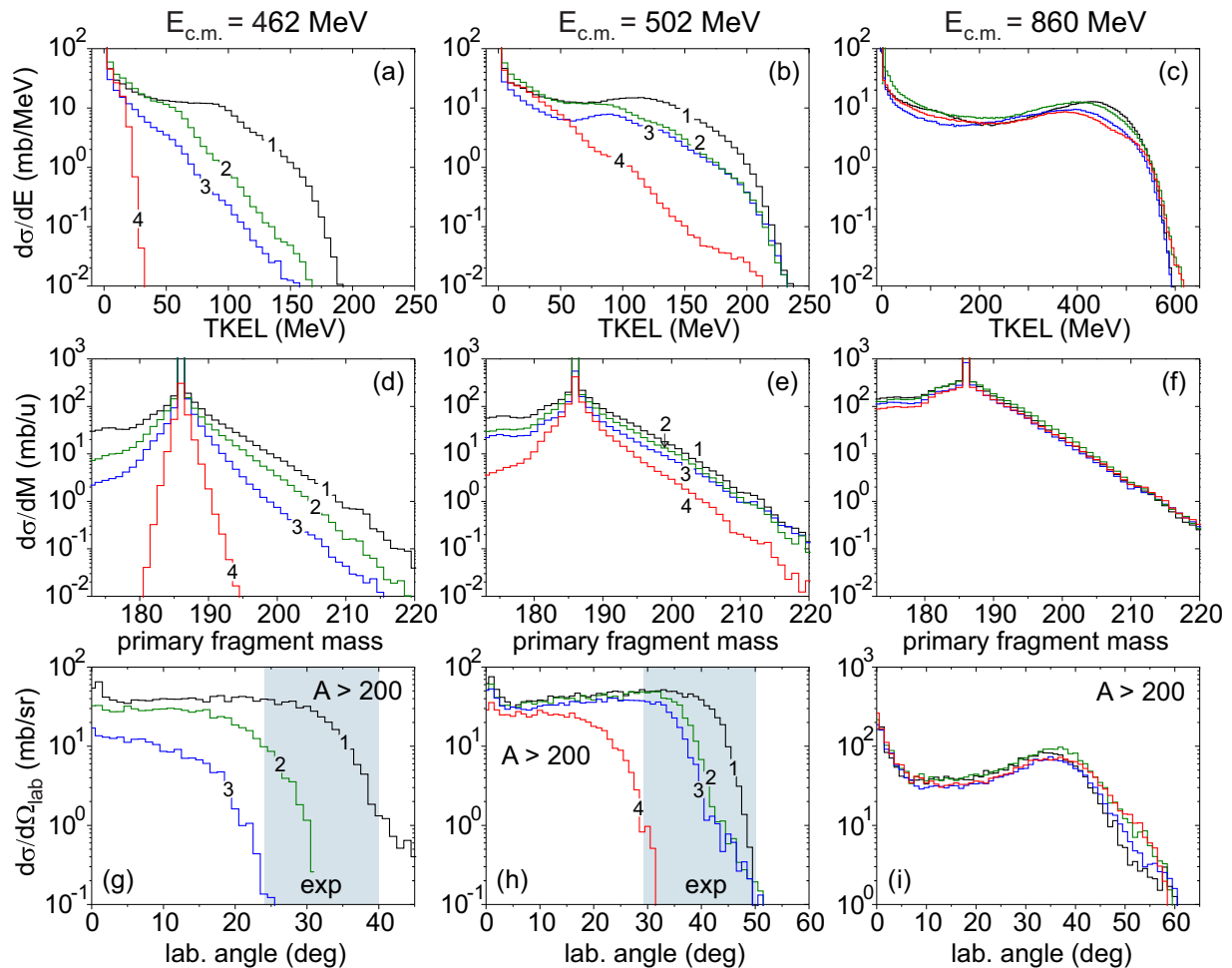


FIG. 4. TKEL, mass, and angular distributions of primary products of the $^{160}\text{Gd} + ^{186}\text{W}$ reaction calculated at three energies $E_{c.m.} = 462$, 502, and 860 MeV. The histograms show the results for tip-to-tip (1), tip-to-side (2), side-to-tip (3), and side-to-side (4) collisions. The shaded areas in the angular distributions show the angular ranges covered in the experiment for detecting TLFs [11].

the influence of mutual orientations of colliding nuclei in absence of SeqF of highly excited reaction products. The differential cross sections of fragments obtained in both reactions were measured under the same experimental conditions. The detectors covered the following angular ranges: $15^\circ \leq \theta_{\text{lab.}} \leq 35^\circ$ and $27^\circ \leq \theta_{\text{lab.}} \leq 47^\circ$. The comparable collision energies $E_{c.m.} = 500$ and 485 MeV were chosen respectively for the $^{144}\text{Sm} + ^{144}\text{Sm}$ and $^{154}\text{Sm} + ^{154}\text{Sm}$ reactions [45,46]. The experimental charge resolution of 1.6 units (FWHM) was taken into account in the calculations.

The angular distributions of final products in the Sm + Sm reactions with total kinetic energy losses (TKEL) larger than 25 MeV are shown in Fig. 2. It is clear that the model provides a good description for the shape and position of the maximum of the distribution for the $^{144}\text{Sm} + ^{144}\text{Sm}$ reaction with spherical nuclei in their ground states. The angular distribution of the fragments obtained in the reaction between the deformed nuclei $^{154}\text{Sm} + ^{154}\text{Sm}$ also agrees reasonably with the data; however, the theoretical width slightly exceeds the experimental results. The shape of the distribution insignificantly suffers from the method that takes into account the orientational effects. Different orientations lead to different

angles of grazing collisions. A more compact side-to-side configuration has a larger grazing angle. The tip-to-side and side-to-tip orientations for this symmetric system lead to the same grazing angle in the center-of-mass frame. The model considers only four different mutual orientations of colliding nuclei. That is why the calculated curve has three maxima corresponding to the tip-to-tip, tip-to-side, and side-to-side collisions. Better results for the angular distribution for the $^{154}\text{Sm} + ^{154}\text{Sm}$ reaction can be achieved by taking into account additional mutual orientations of nuclei in the averaging procedure or by complete consideration of evolution of the orientational degrees of freedom in dynamical calculations.

Another important feature of the reaction dynamics is an increase in nucleon transfer with increased TKEL. It can be seen from Fig. 3 where the charge distributions of the $^{154}\text{Sm} + ^{154}\text{Sm}$ reaction products are plotted for different TKEL values. The experimental data and the calculation results were both scaled for convenient visualization. The calculation results have a Gaussian form and fit well with the experimental data. A certain underestimation of light products with $Z < 62$ is due to the experimental background, which was not completely eliminated during the data

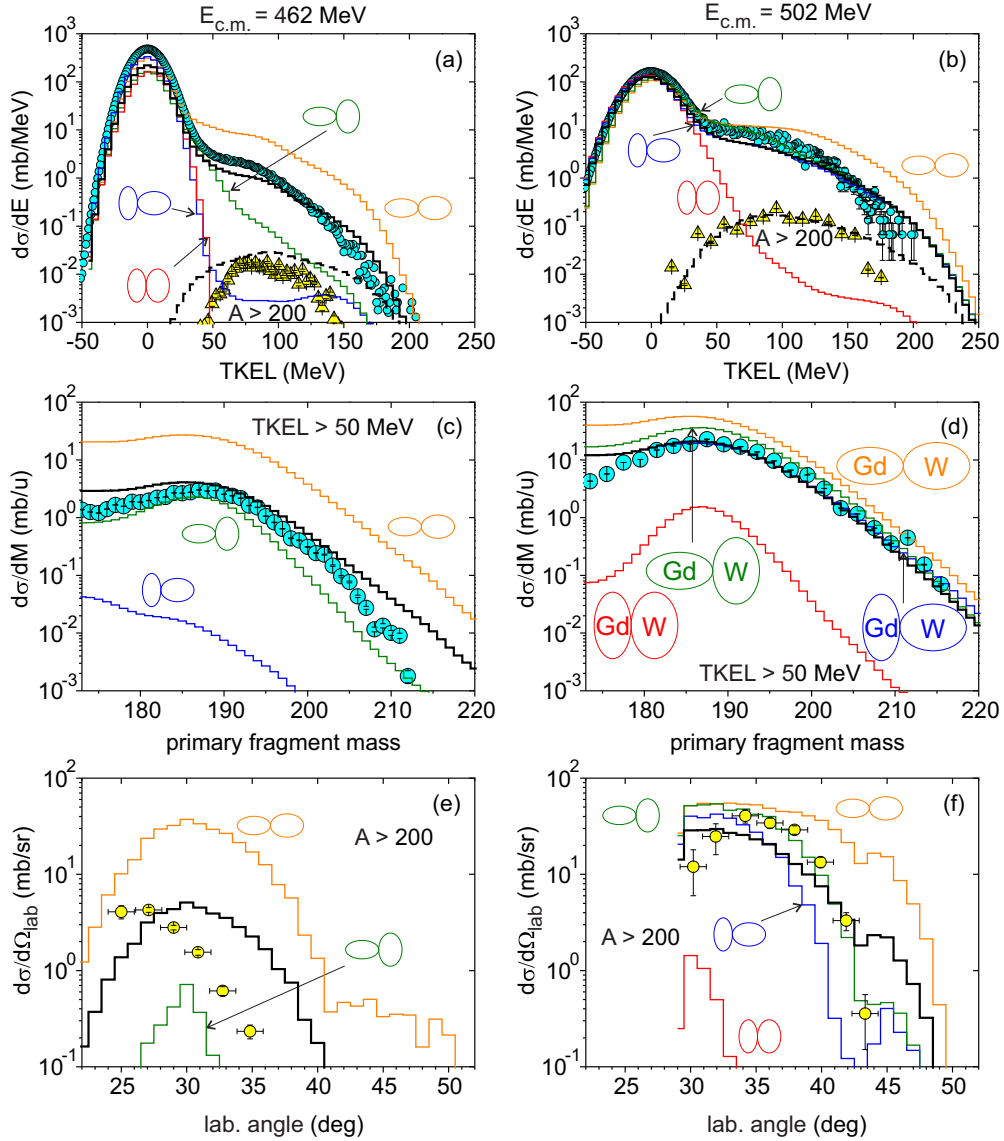


FIG. 5. TKEL, mass, and angular distributions of primary products obtained in the $^{160}\text{Gd} + ^{186}\text{W}$ reaction at two energies $E_{c.m.} = 462$ and 502 MeV. The symbols are the experimental data [11], the thin lines are the calculations for tip-to-tip, side-to-tip, tip-to-side, and side-to-side collisions; the thick lines show the total cross sections averaged over the mutual orientations of the projectile and target nuclei. The angular distributions, as well as the dashed histograms and triangles for the energy distributions, correspond to the TLFs with $A > 200$.

analysis [46]. The calculations predict more symmetrical charge distributions.

B. $^{160}\text{Gd} + ^{186}\text{W}$ system

This approach was applied to the $^{160}\text{Gd} + ^{186}\text{W}$ collisions, where both reaction partners have prolate deformations in the ground state $\beta_2(^{160}\text{Gd}) = 0.28$ and $\beta_2(^{186}\text{W}) = 0.22$ [30]. The experimental data for this reaction have recently been obtained at two near-barrier collision energies $E_{c.m.} = 462$ and 502 MeV [11]. It allows one to study the influence of mutual orientations on the primary TKEL, mass, and angular distributions of the reaction products calculated for the above mentioned energies (see Fig. 4). The angular distributions were calculated for target-like fragments (TLFs) with $A > 200$.

The experimental collision energies are in the same energy range as the calculated Coulomb barriers for different orientations of this system, which are $V_C = 412$ MeV for the tip-to-tip, $V_C = 447$ MeV for the tip-to-side, $V_C = 454$ MeV for the side-to-tip, and $V_C = 492$ MeV for the side-to-side collisions. The strongest influence of the nuclear orientations on the collision dynamics is seen for the lowest energy ($E_{c.m.} = 462$ MeV) corresponding to the barrier for the tip-to-side and side-to-tip configurations. Side-to-side collisions are sub-barrier at this energy. This strongly suppresses the nucleon transfer, as well as the kinetic energy dissipation. The grazing angles and, thus, angular distributions are also significantly affected by the mutual orientations of the colliding nuclei.

The intermediate energy ($E_{c.m.} = 502$ MeV) is just above the barrier for the side-to-side collisions. The distributions of the reaction products become less sensitive to the orientations

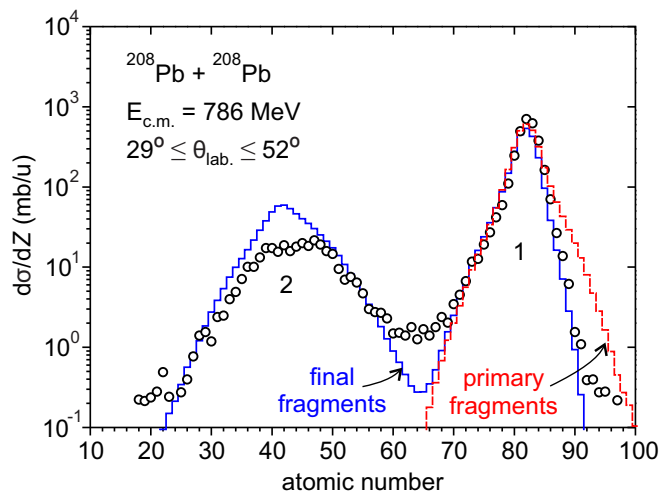


FIG. 6. Charge distribution of final products obtained in the $^{208}\text{Pb} + ^{208}\text{Pb}$ reaction at $E_{c.m.} = 786$ MeV. The dashed and solid histograms represent the calculated distributions of primary and final fragments, respectively. The symbols correspond to the experimental data [47] (scaled, since the data in Ref. [47] are given in arbitrary units). Contributions of DI (1) and SeqF (2) processes to the inclusive charge distribution are shown.

of nuclei. At energies significantly higher than the Coulomb barrier ($E_{c.m.} = 860$ MeV or 10 MeV/u in our case), the orientational effects disappear.

The experiment on the $^{160}\text{Gd} + ^{186}\text{W}$ collisions was done at the double-arm time-of-flight spectrometer CORSET (CORrelation SETup) in Flerov Laboratory of Nuclear Reactions, JINR [11]. The angular ranges $25^\circ \leq \theta_{lab.} \leq 65^\circ$ and $29^\circ \leq \theta_{lab.} \leq 66^\circ$ were covered in the experiment to detect binary reaction products in coincidence at $E_{c.m.} = 462$ and 502 MeV, respectively. The shaded areas in Fig. 4 indicate the angular ranges set for detecting the TLFs. The TKEL, mass, and angular distributions of reaction products obtained in the experiment and the calculated ones are shown in Fig. 5. The calculations were performed for the experimentally covered angular ranges. The experimental energy and mass resolutions (FWHM) of 12 MeV and 3 units were taken into account in the theoretical calculations. A satisfactory overall agreement with the data can be mentioned. However, a certain overestimation of the experimental mass distribution has been observed for the collision energy $E_{c.m.} = 462$ MeV, while a considerably good description has been achieved for $E_{c.m.} = 502$ MeV.

It should be mentioned that the visible growth of the TLFs yields with an increasing energy [Figs. 5(c) and 5(d)] is due to a strong dependence of the orientational effects on the collision energy, which is correctly reproduced by the present model.

C. $^{208}\text{Pb} + ^{208}\text{Pb}$, ^{208}Pb , ^{238}U systems

In collisions of heavy nuclei, the SeqF of highly excited heavy reaction products may play a significant role. It is not always possible to completely distinguish SeqF from the binary products, but it can be done quite reliably for the $^{208}\text{Pb} + ^{208}\text{Pb}$ reaction (see Fig. 6). The products with $Z > 65$ form the main component of the charge distribution

of quasielastic and DI collisions with the position of the maximum at $Z = 82$. The additional component centered at $Z \approx 40$ consists of SeqF fragments having $15 \leq Z \leq 65$. The SeqF process hinders the survival of heavy above-target nuclei, limiting their production in DI collisions.

The $^{208}\text{Pb} + ^{208}\text{Pb}$ reaction products were measured covering the $29^\circ \leq \theta_{lab.} \leq 52^\circ$ angular range at two collision energies $E_{c.m.} = 726$ and 786 MeV [47]. The experimental charge resolution of 2.5 units (FWHM) was taken into account in the calculations. The histograms were normalized to DI events and fit the experimental data rather well. The sequential fission rates were deduced experimentally as a ratio of the missing cross section (due to the SeqF process) to the one for primary products, subtracting the quasielastic events having $\text{TKEL} < 50$ MeV. The found rates for the $^{208}\text{Pb} + ^{208}\text{Pb}$ reaction at collision energies $E_{c.m.} = 726$ and 786 MeV are 11% and 16%, respectively. The corresponding calculated values are 10% and 21%. Obviously, the SeqF probability grows with an increasing collision energy. Therefore, it seems reasonable to use the near-barrier collision energies in order to reduce the SeqF component and to increase the yields of above-target products.

The Coulomb force dominates over the attractive nuclear force in an interaction of two heavy nuclei, such as lead. It results in broad angular distribution of the DI reaction products in contrast to the peaked distribution of the fragments near the grazing angle obtained in the collisions of lighter nuclei, such as $\text{Sm} + \text{Sm}$ (Fig. 2). The emission angles of the $\text{Pb} + \text{Pb}$ reaction fragments continuously increase with increasing TKEL. This behavior is shown in Fig. 7 for the primary reaction products. The angular distributions of fragments for different TKEL values should be symmetric with respect to 90° . The experimental data obtained in the $65^\circ \leq \theta_{c.m.} \leq 95^\circ$ angular range for PLFs were doubled and symmetrically reflected to reproduce the missing component of TLFs.

The angular distributions of fragments with low TKEL have their maxima near the $\theta_{c.m.}^{\text{gr}} \approx 90^\circ$ and 75° grazing angles for collision energies $E_{c.m.} = 726$ and 786 MeV, respectively. The part of the angular distribution corresponding to PLFs shifts to larger angles with increasing TKEL and crosses the symmetric branch for TLFs at $\theta_{c.m.} = 90^\circ$.

The $^{208}\text{Pb} + ^{238}\text{U}$ reaction was investigated under the same experimental conditions as those of $^{208}\text{Pb} + ^{208}\text{Pb}$ [47]. The charge distributions of products of both reactions for different TKEL bins are compared in Fig. 8. For this comparison, the experimental data were integrated over the angular ranges $68^\circ \leq \theta_{c.m.} \leq 90^\circ$ in the case of the $^{208}\text{Pb} + ^{208}\text{Pb}$ reaction and $70^\circ \leq \theta_{c.m.} \leq 102^\circ$ in the case of the $^{208}\text{Pb} + ^{238}\text{U}$ reaction.

The calculations agree well with the experimental data in Fig. 8(a), where the data for a low collision energy are presented. However, it is seen that the calculated cross section maxima are slightly shifted toward the lower atomic numbers for larger TKEL values, while the maxima of the experimental distributions are almost unchanged. It becomes more evident at higher collision energies [Figs. 8(b) and 8(c)]. Since evaporation of protons from the primary fragments is suppressed, this effect is mainly due to the SeqF.

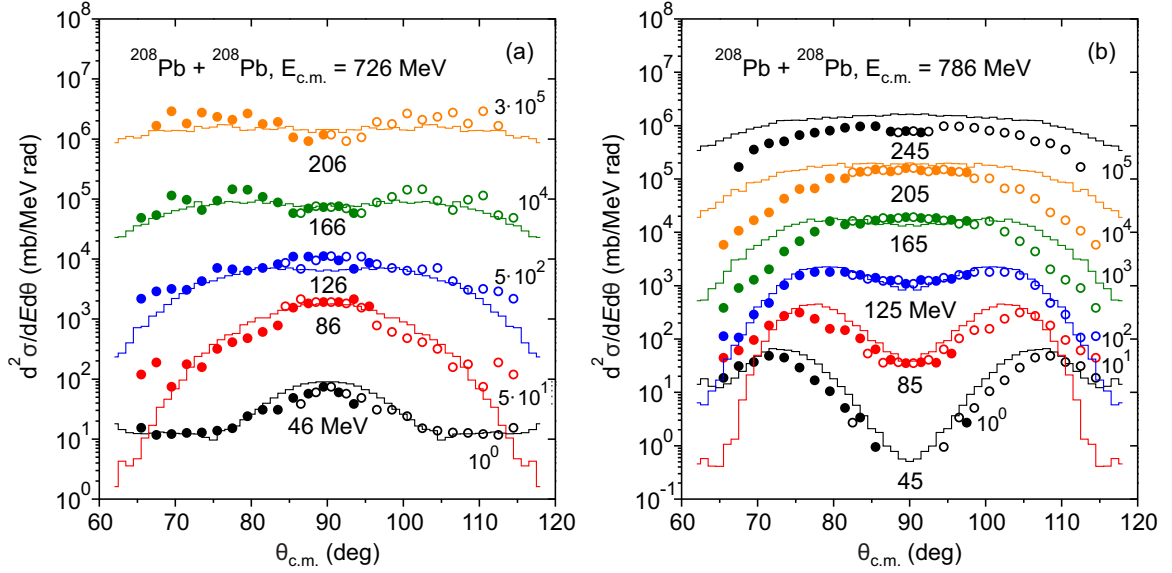


FIG. 7. Angular distributions of primary products for different TKEL bins obtained in the $^{208}\text{Pb} + ^{208}\text{Pb}$ reaction at $E_{c.m.} = 726$ and 786 MeV. The histograms are the calculation results and the symbols correspond to the experimental data [47]. The TKEL bins are 40 MeV wide; their midpoints and multiplication factors are indicated.

D. $^{238}\text{U} + ^{238}\text{U}$, ^{248}Cm , ^{254}Es systems

Collisions of heavy actinides are of particular interest for the developed model. Actinides are deformed in their ground states and their orientations significantly influence the collision dynamics. The problem of synthesis of heavy and superheavy nuclei in DI collisions of actinides has been studied experimentally since the late 1970s for the $^{238}\text{U} + ^{238}\text{U}$, ^{248}Cm reactions [17,18,48]. The fact that the final iso-

topic yields of heavy TLFs obtained in collisions with ^{238}U and ^{248}Cm drop exponentially with an increasing atomic number has been established in a series of these and other works (see, e.g., Ref. [49]). As a rule, the transfer of each proton toward the heavier reaction partner leads to a decrease in the corresponding production cross section by an order of magnitude. The results of our calculations shown in Fig. 9 are in agreement with this trend.

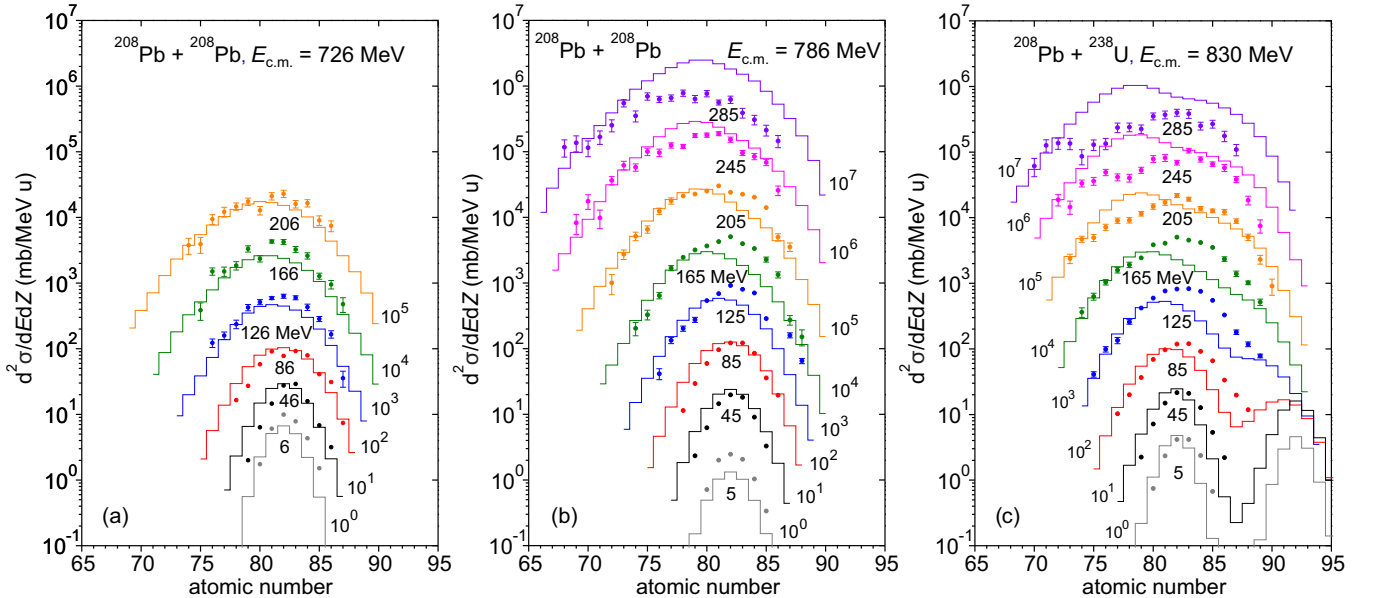


FIG. 8. Charge distributions of final products for different TKEL values obtained in the $^{208}\text{Pb} + ^{208}\text{Pb}$ reaction at $E_{c.m.} = 726$ and 786 MeV [(a), (b)] and the $^{208}\text{Pb} + ^{238}\text{U}$ reaction at $E_{c.m.} = 830$ MeV (c). The energy bins are 40 MeV wide; their midpoints and multiplication factors are indicated. The following angular ranges were considered both in the experimental data and in the calculations: $68^\circ \leq \theta_{c.m.} \leq 90^\circ$ in the case of $^{208}\text{Pb} + ^{208}\text{Pb}$ and $70^\circ \leq \theta_{c.m.} \leq 102^\circ$ in the case of $^{208}\text{Pb} + ^{238}\text{U}$. The experimental data (symbols) are taken from Ref. [47].

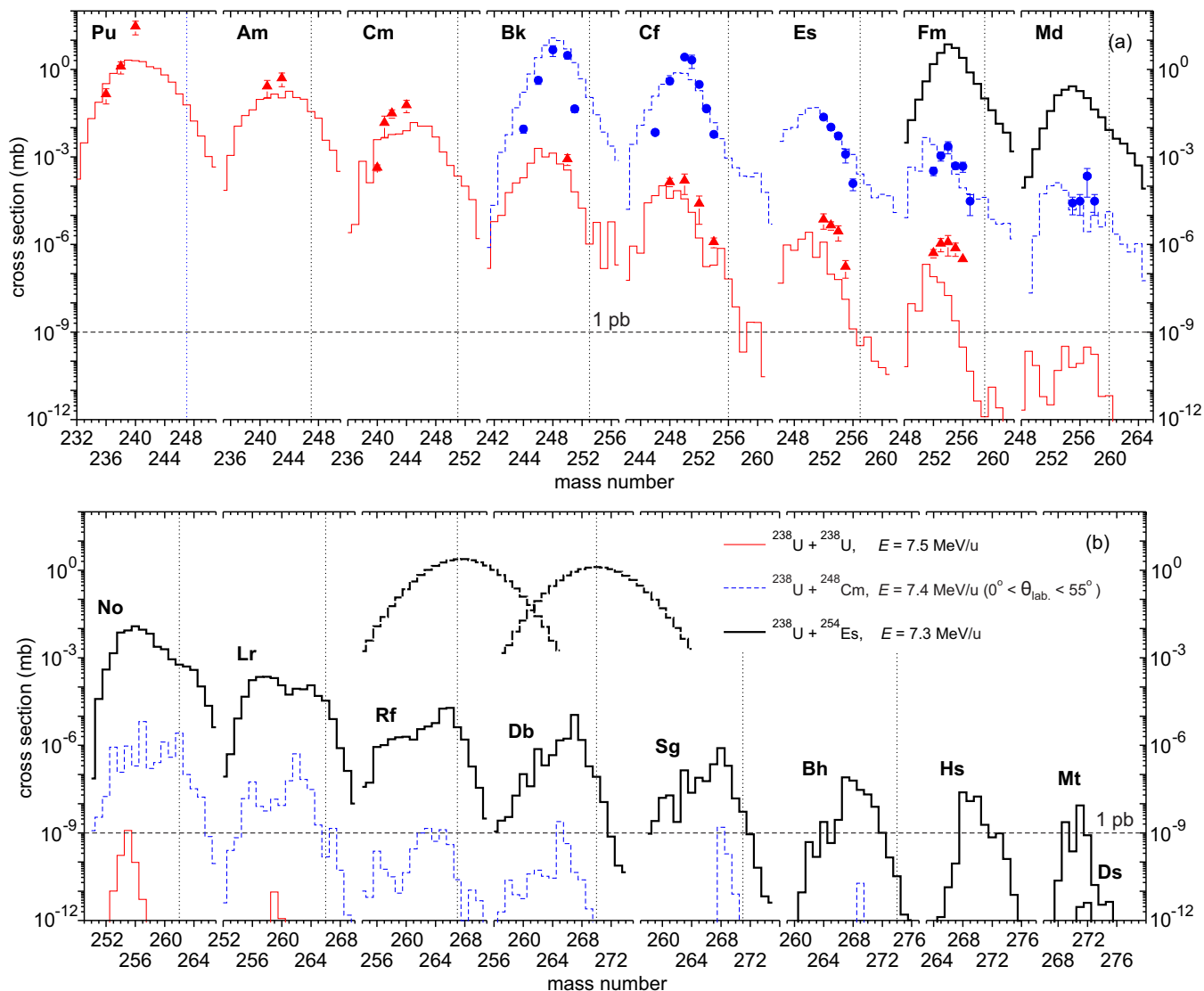


FIG. 9. Isotopic distributions of final above-target products obtained in collisions of actinides. The thin, dashed, and thick histograms correspond to the results of the calculations for the reactions $^{238}\text{U} + ^{238}\text{U}$ ($E = 7.5$ MeV/u), $^{238}\text{U} + ^{248}\text{Cm}$ ($E = 7.4$ MeV/u), and $^{238}\text{U} + ^{254}\text{Es}$ ($E = 7.3$ MeV/u), respectively. The experimental data for the $^{238}\text{U} + ^{238}\text{U}$ reaction (triangles) are taken from Ref. [17], and for $^{238}\text{U} + ^{248}\text{Cm}$ (circles) are from Ref. [18]. For more details, see the text. The heaviest known isotopes of the given chemical elements are indicated by vertical dotted lines. The thick dashed curves show primary isotopic distributions of Rf and Db.

It should be noted that the experimental data shown in Fig. 9 were obtained by radiochemical methods, and a thick target was used in the $^{238}\text{U} + ^{238}\text{U}$ experiment. Hence the final products of the $^{238}\text{U} + ^{238}\text{U}$ reaction shown by triangles in Fig. 9 were detected in the whole angular range for collision energies $E \leq 7.5$ MeV/u. The calculations were performed for a fixed value of $E = 7.5$ MeV/u. The $0^\circ \leq \theta_{\text{lab.}} \leq 55^\circ$ angular range was covered in the experiment on the $^{238}\text{U} + ^{248}\text{Cm}$ collisions at $E = 7.4$ MeV/u [17,18].

A rather good agreement of the calculated and experimental isotopic yields was achieved for the absolute cross section values, and a small shift of the maxima of the calculated distributions toward lower masses can be seen in Fig. 9(a) for the heaviest measured nuclides. Irregularities in the results of the calculations for low cross sections are caused by poor statistics. To improve agreement with the data shown in Fig. 9(a),

one should increase the nucleon transfer rates λ_A^0 and λ_Z^0 responsible, in our model, for the proton and neutron transfer probabilities in the vicinity of the contact point [see Eqs. (5) and (6)]. The required increase should be about two times for the actinide-actinide collisions. Analysis performed for much lighter systems (e.g., $^{40}\text{Ca} + ^{208}\text{Pb}$), which are not discussed here, in contrast requires decreasing the transfer rate coefficients to describe the existing data for the nucleon transfer cross sections. Preliminarily, we found that the transfer rates should depend on the total mass of the system as $\sim A^2/1.2 \times 10^5$. We also found that such a change in the model parameters will not alter noticeably any result or conclusion made in this paper. Moreover, changes in the calculated quantities for lighter (than actinide-actinide) systems studied in this paper are even smaller and nearly invisible. Therefore, we decided not to alter the model parameters fixed in Ref. [7]

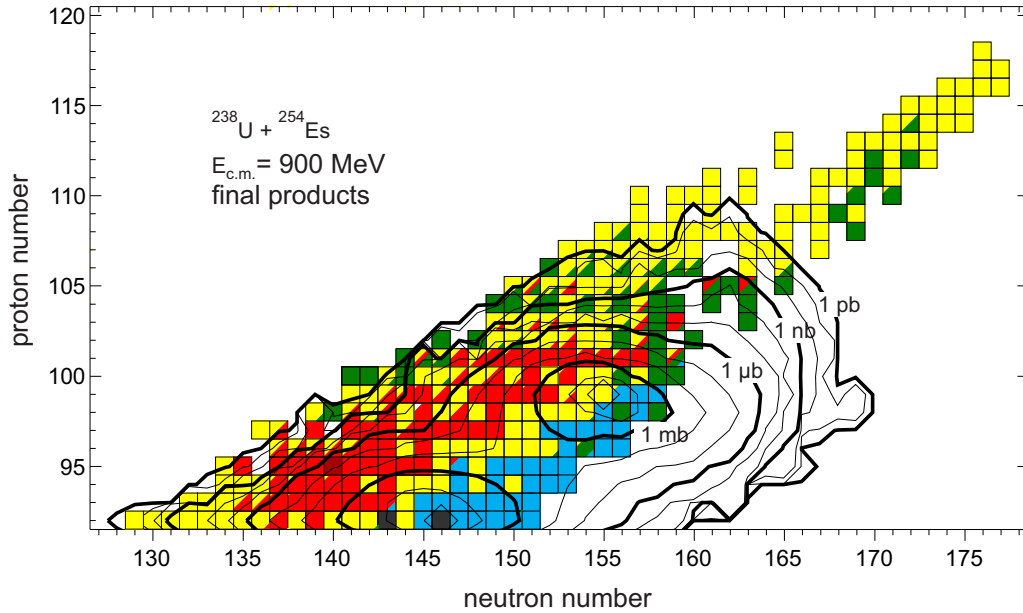


FIG. 10. Production cross sections of final products in the $^{238}\text{U} + ^{254}\text{Es}$ reaction at $E_{\text{c.m.}} = 900$ MeV. The contour lines are drawn over an order of magnitude of the cross section down to 1 pb.

and will consider the necessity of any change after a detailed study of reactions between lighter ions in our forthcoming works.

The production cross sections of nuclei with $Z > 103$ do not exceed 1 pb in the $^{238}\text{U} + ^{248}\text{Cm}$ collisions, which makes synthesis of superheavy elements unreasonable using this reaction. However, in some cases the yields of as yet unknown neutron-enriched isotopes of heavy actinides are sufficiently large for their experimental identification. The vertical dotted lines in Fig. 9 indicate the heaviest known isotopes for each chemical element.

The production cross sections of heavy TLFs for the given Z are approximately four orders of magnitude larger for the $^{238}\text{U} + ^{248}\text{Cm}$ reaction compared with $^{238}\text{U} + ^{238}\text{U}$. It certainly motivates one to use the heaviest available target in order to achieve the largest production cross sections for heavy and superheavy nuclei in DI collisions. We have performed calculations for the $^{238}\text{U} + ^{254}\text{Es}$ reaction as one of the possible combinations with a heavy target (see Figs. 9 and 10). The collision energy was set to $E = 7.3$ MeV/u ($E_{\text{c.m.}} = 900$ MeV), which is slightly above the Coulomb barrier for the side-to-side mutual orientation ($V_C = 874$ MeV). The whole angular range is covered in the calculations, but practically all above-target products are emitted in the forward angles up to $\theta_{\text{lab.}} = 55^\circ$.

The calculations for the $^{238}\text{U} + ^{254}\text{Es}$ reaction predict an additional shoulder for No and Lr isotopic distributions, which becomes a maximum for Rf, Db, and Sg distributions. This phenomenon can be explained by the impact of the $N = 162$ neutron subshell on the formation of final reaction products from the primary ones during the de-excitation process. Note that there is no visible effect of this subshell on the formation of the primary products [compare the primary and final fragments for Rf and Db isotopes in Fig. 9(b)]. The impact of the

$N = 162$ subshell is also present in Db and Sg distributions obtained in the $^{238}\text{U} + ^{248}\text{Cm}$ reaction.

As can be seen from Fig. 9, the yields of primary fragments are rather large. For example, excited $Z = 114$ nuclei can be produced with cross sections of about 1 μb (not shown in Fig. 9). Nevertheless, high excitation energies and angular momenta lead to rather low probabilities of their survival.

The production cross sections for the $^{238}\text{U} + ^{254}\text{Es}$ reaction products with $Z > 91$ are shown in Fig. 10. In this reaction, unknown neutron-enriched isotopes of elements from U to Md can be produced with cross sections exceeding 1 μb . The above-discussed decrease in the isotopic distributions with an increasing atomic number imposes certain restrictions on the formation of above-target nuclei. In particular, the possibility of synthesizing unknown superheavy nuclides in DI collisions of actinides is rather limited.

The initial orientation of statically deformed nuclei also affects the production yields of heavy above-target nuclei. Lower excitation energies of primary fragments formed in more compact side-to-side collisions will increase their survival probability. On the other hand, the cross sections for primary products for the side-to-side collisions are smaller than for other orientations. The final yield is a product of the survival probability and primary cross section. Determination of an optimal collision energy is of great importance for planning experiments on production of heavy nuclei and will be a topic of future studies.

IV. CONCLUSIONS AND OUTLOOK

In this paper, the multinucleon transfer processes in low-energy collisions have been analyzed both for spherical and statically deformed nuclei. The model provided a reasonable agreement between the calculated and the measured energy,

angular, charge, and isotopic distributions of reaction products for a number of MNT reactions with medium-mass and heavy nuclei.

The mutual orientation of colliding statically deformed nuclei in the entrance channel strongly affects the reaction dynamics at near-barrier energies. This applies to the absolute values and widths of the energy, angular, mass, and charge distributions of reaction products obtained for different mutual orientations of projectile and target nuclei. These orientational effects gradually disappear with an increasing collision energy to the values well above the Coulomb barrier for all orientations.

The developed approach allows us to calculate the yields of the above-target nuclei produced in collisions of heavy actinides at near-barrier collision energies. The calculation results show a strong exponential drop in the production cross sections with an increasing atomic number due to high excita-

tion energies and angular momenta of the primary products. This drop was previously observed experimentally for the $^{238}\text{U} + ^{238}\text{U}$, ^{248}Cm reactions [17,18]. This fact makes the region of new superheavy nuclides hardly reachable in MNT reactions. However, there is a real chance to produce a number of neutron-enriched isotopes of heavy actinides with cross sections exceeding $1\ \mu\text{b}$ in the MNT reaction with a ^{254}Es target.

Both theoretical and experimental studies of the energy dependence of the production yields of heavy neutron-enriched nuclei in MNT reactions with heavy ions is of particular interest for determining the conditions for their synthesis.

ACKNOWLEDGMENTS

One of us (V.V.S.) has been supported by the JINR Grant for Young Scientists and Specialists No. 18-502-08.

-
- [1] A. G. Artukh, G. F. Gridnev, V. L. Mikheev, V. V. Volkov, and J. Wilczynski, Transfer reactions in the interaction of $^{40}\text{Ar} + ^{232}\text{Th}$, *Nucl. Phys. A* **215**, 91 (1973).
- [2] C. H. Dasso, G. Pollarolo, and A. Winther, Systematics of Isotope Production with Radioactive Beams, *Phys. Rev. Lett.* **73**, 1907 (1994).
- [3] R. Broda, Spectroscopic studies with the use of deep-inelastic heavy-ion reactions, *J. Phys. G: Nucl. Part. Phys.* **32**, R151 (2006).
- [4] V. Zagrebaev and W. Greiner, Shell effects in damped collisions: A new way to superheavies, *J. Phys. G: Nucl. Part. Phys.* **34**, 2265 (2007).
- [5] V. Zagrebaev and W. Greiner, New way for the production of heavy neutron-rich nuclei, *J. Phys. G: Nucl. Part. Phys.* **35**, 125103 (2008).
- [6] L. Corradi, G. Pollarolo, and S. Szilner, Multinucleon transfer processes in heavy-ion reactions, *J. Phys. G: Nucl. Part. Phys.* **36**, 113101 (2009).
- [7] A. V. Karpov and V. V. Saiko, Modeling near-barrier collisions of heavy ions based on a Langevin-type approach, *Phys. Rev. C* **96**, 024618 (2017).
- [8] E. M. Kozulin, E. Vardaci, G. N. Knyazheva, A. A. Bogachev, S. N. Dmitriev, I. M. Itkis, M. G. Itkis, A. G. Knyazev, T. A. Loktev, K. V. Novikov, E. A. Razinkov, O. V. Rudakov, S. V. Smirnov, W. Trzaska, and V. I. Zagrebaev, Mass distributions of the system $^{136}\text{Xe} + ^{208}\text{Pb}$ at laboratory energies around the Coulomb barrier: A candidate reaction for the production of neutron-rich nuclei at $N = 126$, *Phys. Rev. C* **86**, 044611 (2012).
- [9] J. S. Barrett, W. Loveland, R. Yanez, S. Zhu, A. D. Ayangeakaa, M. P. Carpenter, J. P. Greene, R. V. F. Janssens, T. Lauritsen, E. A. McCutchan *et al.*, $^{136}\text{Xe} + ^{208}\text{Pb}$ reaction: A test of models of multinucleon transfer reactions, *Phys. Rev. C* **91**, 064615 (2015).
- [10] Y. X. Watanabe, Y. H. Kim, S. C. Jeong, Y. Hirayama, N. Imai, H. Ishiyama, H. S. Jung, H. Miyatake, S. Choi, J. S. Song *et al.*, Pathway for the Production of Neutron-Rich Isotopes Around the $N = 126$ Shell Closure, *Phys. Rev. Lett.* **115**, 172503 (2015).
- [11] E. M. Kozulin, V. I. Zagrebaev, G. N. Knyazheva, I. M. Itkis, K. V. Novikov, M. G. Itkis, S. N. Dmitriev, I. M. Harca, A. E. Bondarchenko, A. V. Karpov *et al.*, Inverse quasifission in the reactions $^{156,160}\text{Gd} + ^{186}\text{W}$, *Phys. Rev. C* **96**, 064621 (2017).
- [12] A. Iwamoto, P. Möller, J. R. Nix, and H. Sagawa, Collisions of deformed nuclei: A path to the far side of the superheavy island, *Nucl. Phys. A* **596**, 329 (1996).
- [13] D. J. Hinde, M. Dasgupta, J. R. Leigh, J. C. Mein, C. R. Morton, J. O. Newton, and H. Timmers, Conclusive evidence for the influence of nuclear orientation on quasifission, *Phys. Rev. C* **53**, 1290 (1996).
- [14] K. Nishio, H. Ikezoe, S. Mitsuoka, and J. Lu, Fusion of deformed nuclei in the reactions of $^{76}\text{Ge} + ^{150}\text{Nd}$ and $^{28}\text{Si} + ^{198}\text{Pt}$ at the Coulomb barrier region, *Phys. Rev. C* **62**, 014602 (2000).
- [15] S. Mitsuoka, H. Ikezoe, K. Nishio, and J. Lu, Sub-barrier fusion of deformed nuclei in $^{60}\text{Ni} + ^{154}\text{Sm}$ and $^{32}\text{S} + ^{182}\text{W}$ reactions, *Phys. Rev. C* **62**, 054603 (2000).
- [16] V. Saiko and A. Karpov, Dynamics of near-barrier collisions of statically deformed nuclei, *Acta Phys. Pol. B* **49**, 307 (2018).
- [17] M. Schädel, J. V. Kratz, H. Ahrens, W. Bröchle, G. Franz, H. Gäggeler, I. Warnecke, G. Wirth, G. Herrmann, N. Trautmann, and M. Weis, Isotope Distributions in the Reaction of ^{238}U with ^{238}U , *Phys. Rev. Lett.* **41**, 469 (1978).
- [18] M. Schädel, W. Bröchle, H. Gäggeler, J. V. Kratz, K. Sümmerner, G. Wirth, G. Herrmann, R. Stakemann, G. Tittel, N. Trautmann *et al.*, Actinide Production in Collisions of ^{238}U with ^{248}Cm , *Phys. Rev. Lett.* **48**, 852 (1982).
- [19] C. Golabek, S. Heinz, W. Mittig, F. Rejmund, A. C. C. Villari, S. Bhattacharyya, D. Boilley, G. De France, A. Drouart, L. Gaudefroy *et al.*, Investigation of deep inelastic reactions in $^{238}\text{U} + ^{238}\text{U}$ at Coulomb barrier energies, *Eur. Phys. J. A* **43**, 251 (2010).
- [20] V. I. Zagrebaev, A. V. Karpov, I. N. Mishustin, and W. Greiner, Production of heavy and superheavy neutron-rich nuclei in neutron capture processes, *Phys. Rev. C* **84**, 044617 (2011).
- [21] K. Zhao, Z. Li, X. Wu, and Y. Zhang, Production probability of superheavy fragments at various initial deformations and orientations in the $^{238}\text{U} + ^{238}\text{U}$ reaction, *Phys. Rev. C* **88**, 044605 (2013).

- [22] K. Zhao, Z. Li, Y. Zhang, N. Wang, Q. Li, C. Shen, Y. Wang, and X. Wu, Production of unknown neutron-rich isotopes in $^{238}\text{U} + ^{238}\text{U}$ collisions at near-barrier energy, *Phys. Rev. C* **94**, 024601 (2016).
- [23] Z.-Q. Feng, G.-M. Jin, and J.-Q. Li, Production of heavy isotopes in transfer reactions by collisions of $^{238}\text{U} + ^{238}\text{U}$, *Phys. Rev. C* **80**, 067601 (2009).
- [24] J. Maruhn and W. Greiner, The asymmetric two center shell model, *Z. Phys.* **251**, 431 (1972).
- [25] P. Fröbrich and I. I. Gontchar, Langevin description of fusion, deep-inelastic collisions, and heavy-ion-induced fission, *Phys. Rep.* **292**, 131 (1998).
- [26] G. D. Adeev, A. V. Karpov, P. N. Nadtochii, and D. V. Vanin, Multidimensional stochastic approach to the fission dynamics of excited nuclei, *Phys. Part. Nucl.* **36**, 378 (2005).
- [27] A. B. Migdal, *Theory of Finite Fermi Systems and Applications to Atomic Nuclei* (Interscience, New York, 1967).
- [28] V. Zagrebaev, A. Karpov, Y. Aritomo, M. Naumenko, and W. Greiner, Potential energy of a heavy nuclear system in fusion-fission processes, *Phys. Part. Nuclei* **38**, 469 (2007).
- [29] A. V. Karpov, A. P. Alekseev, M. A. Naumenko, V. A. Rachkov, V. V. Samarin, V. I. Zagrebaev, A. S. Denikin, and V. V. Saiko, NRV web knowledge base on low-energy nuclear physics <http://nrv.jinr.ru>.
- [30] P. Möller, A. J. Sierk, T. Ichikawa, and H. Sagawa, Nuclear ground-state masses and deformations: Frdm(2012), *At. Data Nucl. Data Tables* **109**, 1 (2016).
- [31] V. M. Strutinsky, Shell effects in nuclear masses and deformation energies, *Nucl. Phys. A* **95**, 420 (1967).
- [32] V. M. Strutinsky, Shells in deformed nuclei, *Nucl. Phys. A* **122**, 1 (1968).
- [33] K. T. R. Davies, A. J. Sierk, and J. R. Nix, Effect of viscosity on the dynamics of fission, *Phys. Rev. C* **13**, 2385 (1976).
- [34] A. J. Sierk and J. R. Nix, Fission in a wall-and-window one-body-dissipation model, *Phys. Rev. C* **21**, 982 (1980).
- [35] A. V. Karpov and G. D. Adeev, Langevin description of charge fluctuations in fission of highly excited nuclei, *Eur. Phys. J. A* **14**, 169 (2002).
- [36] V. Zagrebaev and W. Greiner, Unified consideration of deep inelastic, quasi-fission and fusion-fission phenomena, *J. Phys. G: Nucl. Part. Phys.* **31**, 825 (2005).
- [37] W. von Oertzen, H. G. Bohlen, B. Gebauer, R. Künkel, F. Pühlhofer, and D. Schüll, Quasi-elastic neutron transfer and pairing effects in the interaction of heavy nuclei, *Z. Phys. A* **326**, 463 (1987).
- [38] A. V. Karpov, A. S. Denikin, A. P. Alekseev, V. I. Zagrebaev, V. A. Rachkov, M. A. Naumenko, and V. V. Saiko, NRV web knowledge base on low-energy nuclear physics, *Phys. At. Nucl.* **79**, 749 (2016).
- [39] A. V. Karpov, A. S. Denikin, M. A. Naumenko, A. P. Alekseev, V. A. Rachkov, V. V. Samarin, V. V. Saiko, and V. I. Zagrebaev, NRV web knowledge base on low-energy nuclear physics, *Nucl. Instr. Methods Phys. Res. Sect. A* **859** (Suppl. C), 112 (2017).
- [40] A. V. Karpov, V. A. Rachkov, and V. V. Saiko, Formation of neutron-enriched heavy and superheavy nuclei in fusion reactions, *Phys. Part. Nuclei Lett.* **15**, 247 (2018).
- [41] K.-H. Schmidt, B. Jurado, C. Amouroux, and C. Schmitt, General description of fission observables: GEF model code, *Nucl. Data Sheets* **131** (Suppl. C), 107 (2016).
- [42] M. G. Itkis and A. Y. Rusanov, The fission of heated nuclei in reactions involving heavy ions: Static and dynamical aspects, *Phys. Part. Nuclei* **29**, 160 (1998).
- [43] V. E. Oberacker, A. S. Umar, and C. Simenel, Dissipative dynamics in quasifission, *Phys. Rev. C* **90**, 054605 (2014).
- [44] A. S. Umar, V. E. Oberacker, and C. Simenel, Fusion and quasi-fission dynamics in the reactions $^{48}\text{Ca} + ^{249}\text{Bk}$ and $^{50}\text{Ti} + ^{249}\text{Bk}$ using a time-dependent Hartree-Fock approach, *Phys. Rev. C* **94**, 024605 (2016).
- [45] E. C. Wu, K. D. Hildenbrand, H. Freiesleben, A. Gobbi, A. Olmi, H. Sann, and U. Lynen, Influence of Shell Structure on Neutron and Proton Exchange in the Reactions of ^{144}Sm on ^{144}Sm and ^{154}Sm on ^{154}Sm , *Phys. Rev. Lett.* **47**, 1874 (1981).
- [46] K. D. Hildenbrand, H. Freiesleben, A. Gobbi, U. Lynen, A. Olmi, H. Sann, and E. C. Wu, On the influence of shell structure in dissipative collisions, *Nucl. Phys. A* **405**, 179 (1983).
- [47] T. Tanabe, R. Bock, M. Dakowski, A. Gobbi, H. Sann, H. Stelzer, U. Lynen, A. Olmi, and D. Pelte, The Pb-Pb collision, *Nucl. Phys. A* **342**, 194 (1980).
- [48] J. V. Kratz, W. Bröchle, H. Folger, H. Gaggeler, M. Schadel, K. Sümmerer, G. Wirth, N. Greulich, G. Herrmann, U. Hickmann *et al.*, Search for superheavy elements in damped collisions between ^{238}U and ^{248}Cm , *Phys. Rev. C* **33**, 504 (1986).
- [49] D. C. Hoffman, M. M. Fowler, W. R. Daniels, H. R. von Gunten, D. Lee, K. J. Moody, K. Gregorich, R. Welch, G. T. Seaborg, W. Bröchle *et al.*, Excitation functions for production of heavy actinides from interactions of ^{40}Ca and ^{48}Ca ions with ^{248}Cm , *Phys. Rev. C* **31**, 1763 (1985).